Supporting Information

Hierarchical carbon-supported iron carbide derived from zinc-iron bimetallic coordination polymer as an efficient electrocatalyst for alkaline oxygen evolution

Tianlong Cao[a,b,c,d,1,*], Yanfang Li[a,1], Jianguo Zhao[a,d], Qihui Jiao[a], Wenjie Chuai[e], Xuefei Zhang[f], Zuopeng Li[e], Mingjun Pang[a,d,*]

a Engineering Research Center of Coal-Based Ecological Carbon Sequestration Technology of the Ministry of Education, Shanxi Datong University, Datong 037009, China.
b Institute of Coal Chemistry, Chinese Academy of Sciences, Taiyuan 030001, China.
c Northwest Yongxin Coating Limited Company, Lanzhou 730046, China.
d Key Laboratory of Graphene Forestry Application of National Forest and Grass Administration, Shanxi Datong Universtiy, Datong 037009, China.
e School of Chemistry and Chemical Engineering, Shanxi Datong University, Datong 037009, China.
f Qingyuan Innovation Laboratory, Quanzhou 362801, China.

1 These authors contributed equally to this work.
* Correspondence: tianlong230228@163.com; pangmingjun3714@163.com.

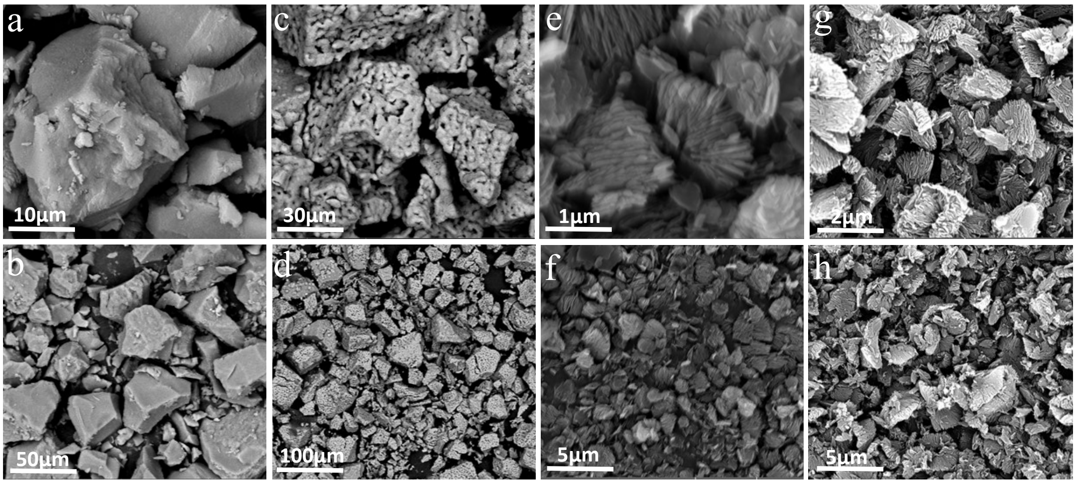

Figure S1 SEM images of (a-b) Fe-CP, (c-d) Fe/C-900, (e-f) Zn-CP and (g-h) Zn/C-900.

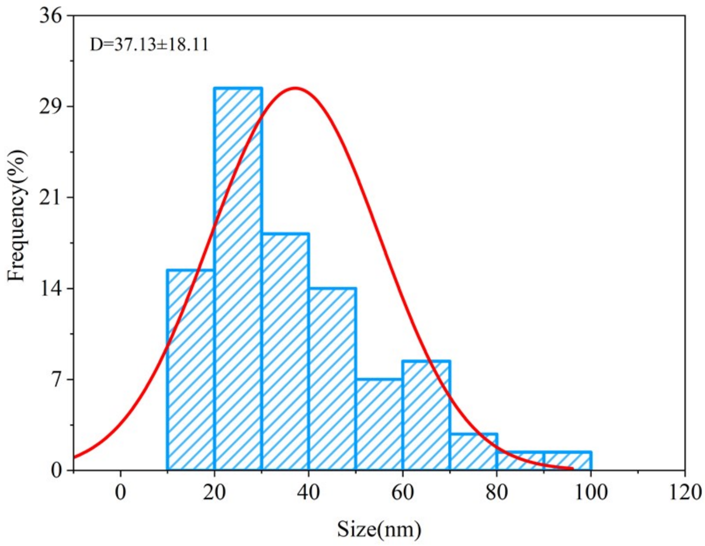

Figuere S2 Particle size distribution of Fe_3C on ZnFe(3:1)/C-900 catalyst.

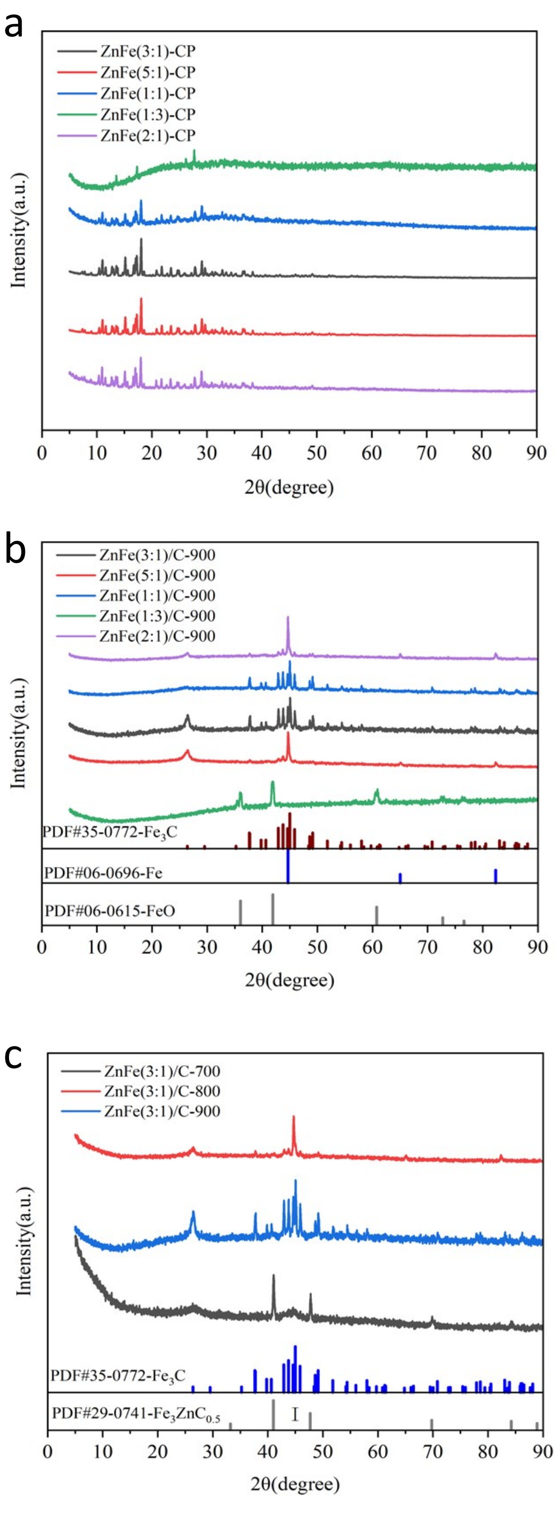

Figure S3 (a) XRD patterns of ZnFe(3:1)-CP, ZnFe(5:1)-CP, ZnFe(1:1)-CP, ZnFe(1:3)-CP and ZnFe(2:1)-CP; (b) XRD patterns of ZnFe(3:1)/C-900, ZnFe(5:1)/C-900, ZnFe(1:1)/C-900, ZnFe(1:3)/C-900 and ZnFe(2:1)/C-900; (c) XRD patterns of ZnFe(3:1)/C-700, ZnFe(3:1)/C-800 and ZnFe(3:1)/C-900.

Table S1 Atomic percentage content and mass percentage content of ZnFe(3:1)/C-900 catalyst surface elements.

Elements	Atom/%	Mass/%
C	91.25	86.28
N	2.86	3.15
O	4.93	6.22
Fe	0.8	3.53
Zn	0.16	0.82

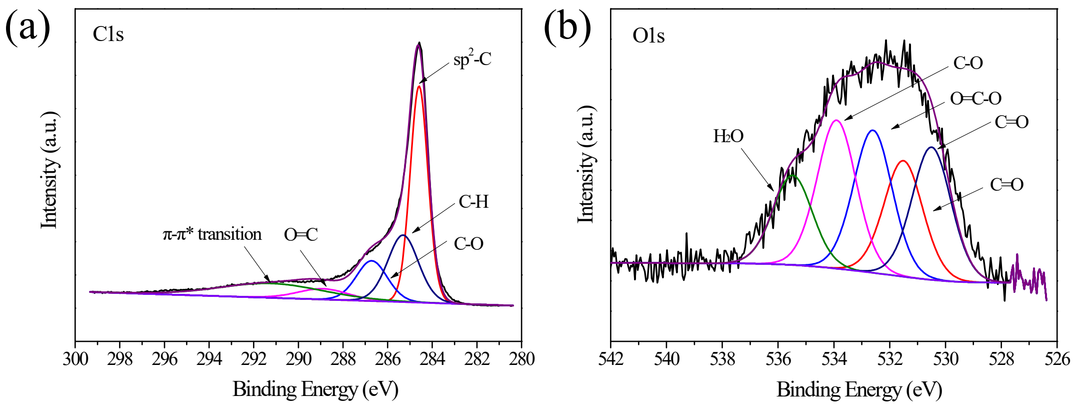

Figure S4 Deconvolution curves of (e) C1s and (b) O1s XPS fine spectra for ZnFe(3:1)/C-900 catalyst.

Table S2 Performance comparison of commercial RuO_2 and IrO_2 catalysts versus several carbon supported iron-based catalysts for alkaline OER.

Sample	Overpotential (mV)	Tafel slope (mV/dec)	Stability (h)	Electrolyte	Ref.
Commercial RuO_2	310 mV@10mA/cm^2	49.2	<1	1.0 M KOH	[1]
Commercial IrO_2	320 mV@10mA/cm^2	70	<3	0.1 M KOH	[2]
B-C_3N_4@Fe_3C	243 mV@10mA/cm^2	38.2	32	1.0 M KOH	[3]
FeSAs-PFN-CNTs	310 mV@10mA/cm^2	63.8	24	1.0 M KOH	[4]
Fe/Ni_3.0h	310 mV@10mA/cm^2	37	10	1.0 M KOH	[5]
Fe_3C@CNF/NC-950	311 mV@10mA/cm^2	63	16	1.0 M KOH	[6]
Co/FeC@NHC-1	380 mV@10mA/cm^2	70	11	1.0 M KOH	[7]
Fe_3C/$CoFe_2O_4$@CNFs-1.5	340 mV@10mA/cm^2	128.4	8	0.1 M KOH	[8]
Fe_3C@CNTs	375 mV@20mA/cm^2	120	4	1.0 M KOH	[9]
Fe_3C@NG800-0.2	361 mV@10mA/cm^2	62	20	0.1 M KOH	[10]
$NiFe_3$@NGHS-NCNTs	383 mV@10mA/cm^2	136.13	15	0.1 M KOH	[11]
Fe_3S_4/NF	257 mV@10mA/cm^2	45.9	12	1.0 M KOH	[12]
FNC@PANi NCs	219 mV@10mA/cm^2	108.7	10	1.0 M KOH	[13]
ZnFe(3:1)/C-900	408 mV@10mA/cm^2	76.1	15	1.0 M KOH	This work

Reference

[1] J. C. Ma, X. J. Bai, W. X. He, S. Wang, L. L. Li, H. Chen, T. Q. Wang, X. M. Zhang, Y. N. Li, L. Y. Zhang, J. Y. Chen, F. B. Meng, Y. Fu. Amorphous FeNi-bimetallic infinite coordination polymers as advanced electrocatalysts for the oxygen evolution reaction. Chem. Commun., 2019, 55, 12567-12570.

[2] Y. Song, T. Y. Tian, C. M. Li, X. Zeng, S. Zhang, L. Chen, Z. H. Yang, Q. Z. Ji, X. L. Zhao, F. Y. Chen. Controlled fabrication of Fe_3N@NG composites as superior oxygen evolution reaction electrocatalysts. Carbon Resour. Convers. 2024, 7, 100207.

[3] G. P. Yang, T. X. Yang, Z. G. Wang, K. Wang, M. M. Zhang, P. D. Lund, S. N. Yun. Targeted doping induces interfacial orientation for constructing surface-functionalized Schottky junctions to coordinate redox reactions in water electrolysis. Adv. Powder Mater., 2024, 3, 100224.

[4] M. Ramadoss, H. S. Yu, A. Rajkamal, G. J. Yun, Z. H. Zhang, C. T. Yang, F. Ma, Y Wu, Q. Chen, Y. F. Chen. Fe-single-atom-coupled Fe_3C multifunctional catalysts on P-, F-, N-doped carbon nanotubes for stable Zn–air batteries with ultra-high power densities. J. Mater. Chem. A, 2024, 12, 30798-30809.

[5] A. G. Dymerska, K. Wenelska, A. L. Zinnatullin, R. Zairov, E. Mijowska. Electroactive heterojunctions of iron-based compounds in oxygen evolution reaction-Insight into synergy and mechanism. Electrochimica Acta, 2024, 482, 144005.

[6] X. E. Gao, G. Kao, J. Yu. Fe_3C nanoparticles and carbon nanofiber decorated N-doped carbon framework for bifunctional water splitting. Digest Journal of Nanomaterials and

Biostructures, 2021, 16, 601-612.
[7] Q. Zhang, M. X. Fu, G. Y. Ning, Y. N. Sun, H. Y. Wang, X. Y. Fan, H. J. Lu, Y. F. Zhang, H. Wang. Co/FeC core–nitrogen doped hollow carbon shell structure with tunable shell-thickness for oxygen evolution reaction. J. Colloid Interface Sci., 2020, 580, 794-802.
[8] Y. B. Sun, Y. Li, S. J. You, X. R. Li, Y. Zhang, Z. Cai, M. Y. Liu, N. Q. Ren, J. L. Zou. $Fe_3C/CoFe_2O_4$ nanoparticles wrapped in one-dimensional MIL-53 (Fe)-derived carbon nanofibers as efficient dual-function oxygen catalysts. Chem. Eng. J., 2021, 424, 130460.
[9] M. Wang, Y. Zhang, T. Peng, M. Kumar, Q. T. Zhang, W. Zhao. Endohedral Fe_3C decorated multi-walled CNTs as an efficient electrocatalyst for oxygen evolution. Diam. Relat. Mater., 2021, 118, 108508.
[10] H. L. Jiang, Y. F. Yao, Y. H. Zhu, Y. Y. Liu, Y. H. Su, X. L. Yang, C. Z. Li. Iron Carbide Nanoparticles Encapsulated in Mesoporous Fe-N-Doped Graphene-Like Carbon Hybrids as Efficient Bifunctional Oxygen Electrocatalysts. ACS Appl. Mater. Interfaces, 2015, 7, 38, 21511-21520.
[11] Y. F. Ma, W. H. Chen, Z. Q. Jiang, X. N. Tian, X. Y. Wang, G. L. Chen, Z. J. Jiang. NiFe nanoparticles supported on N-doped graphene hollow spheres entangled with self-grown N-doped carbon nanotubes for liquid electrolyte/flexible all-solid-state rechargeable zinc–air batteries. J. Mater. Chem. A, 2022, 10, 12616-12631.
[12] A. Kundu, B. Kumar, B. Chakraborty. Greigite Fe_3S_4-Derived α-FeO(OH) Promotes Slow O−O Bond Formation in the Second-Order Oxygen Evolution Reaction Kinetics. J. Phys. Chem. C 2022, 126, 16172−16186.
[13] A. K. Kakarla, H. Bandi, R. Shanthappa, W. Syed, T Wang, J. S. Yu. Polyaniline layered N-doped carbon-coated iron oxide nanocapsules for extremely active Li-ion battery anode and oxygen evolution reaction. Carbon, 2024, 228, 119308.

Table S3 Elemental reaction pathway of the Krasil'shchikov mechanism model for Metal Catalysts in the OER (M: Metal; *: Transition state).

Equation	Tafel slope (mV/dec)	Number
$M^* + OH^- \leftrightarrow M^*O\text{-}H + e^-$	120	1
$M^*O\text{-}H + OH^- \leftrightarrow M^*O^- + H_2O$	60	2
$M^*O^- \rightarrow M^*O + e^-$	45	3
$2\,M^*O \rightarrow M^* + O_2$	15	4

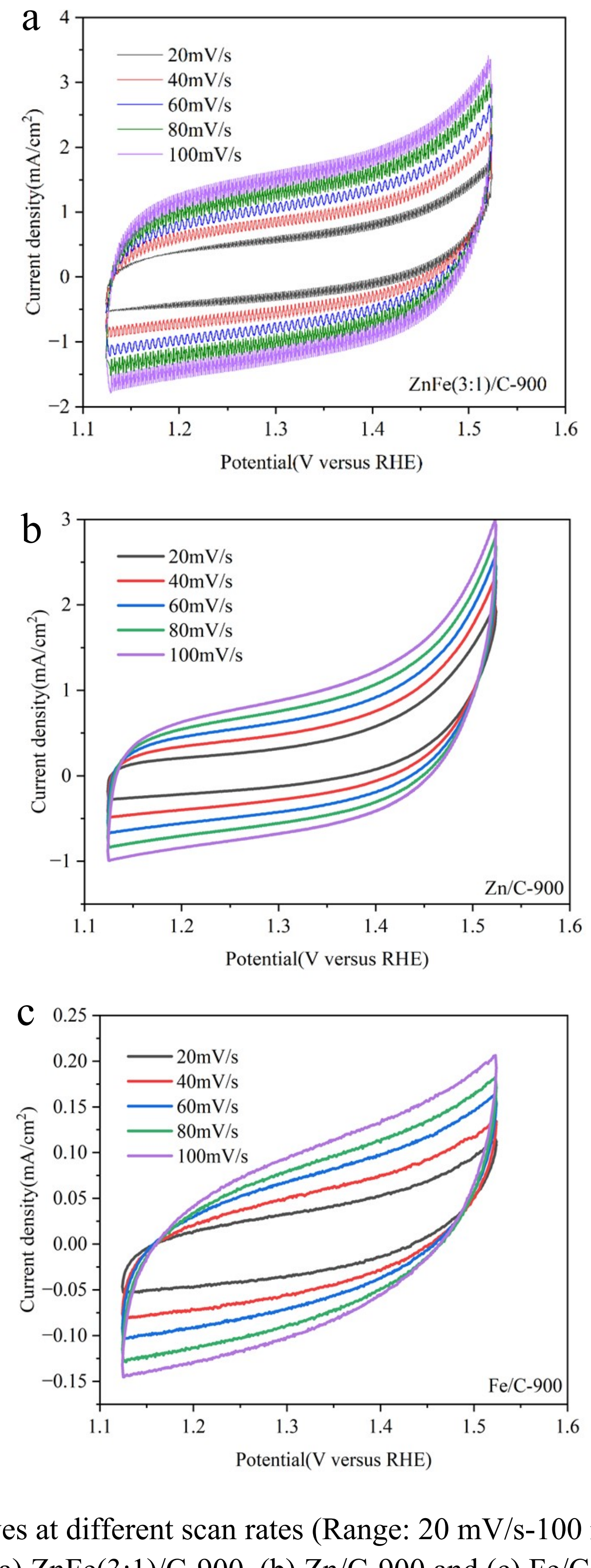

Figure S5 CV curves at different scan rates (Range: 20 mV/s-100 mV/s, Step length: 20 mV/s) for (a) ZnFe(3:1)/C-900, (b) Zn/C-900 and (c) Fe/C-900 samples.

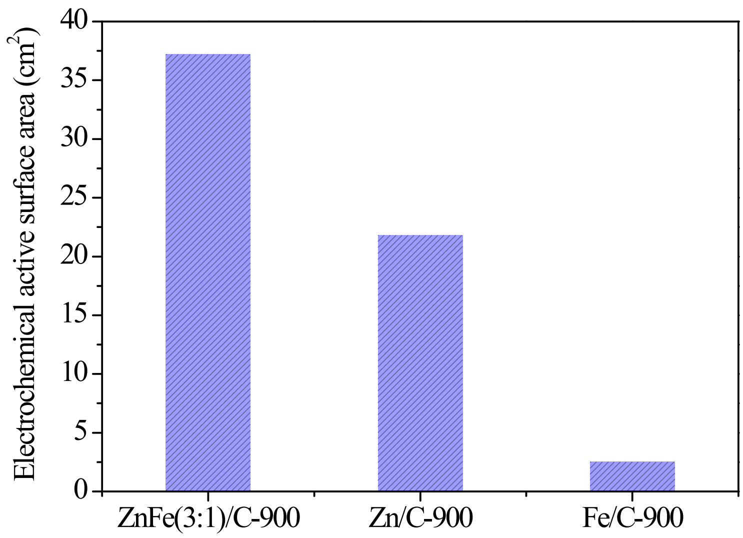

Figure S6 ECSA comparison of ZnFe(3:1)/C-900, Zn/C-900, and Fe/C-900 catalysts.

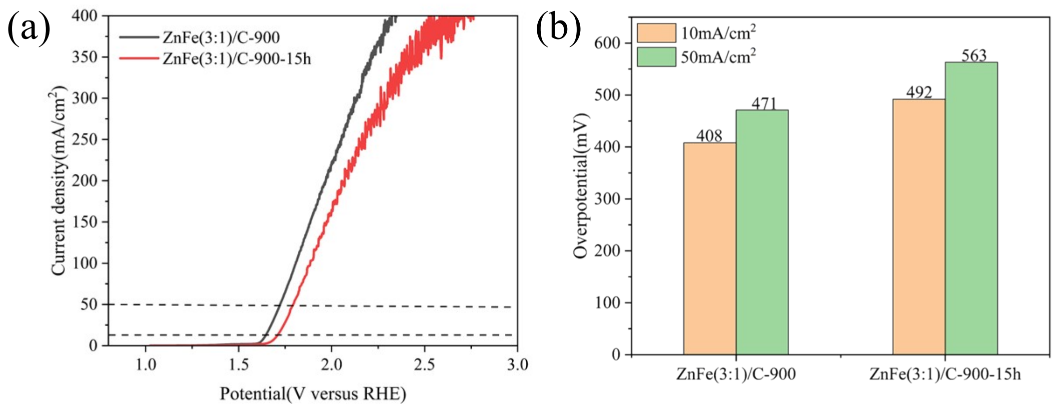

Figure S7 LSV comparison and overpotential values of ZnFe(3:1)/C-900 catalyst at 10 mA/cm^2 and 50 mA/cm^2 before and after stability testing.

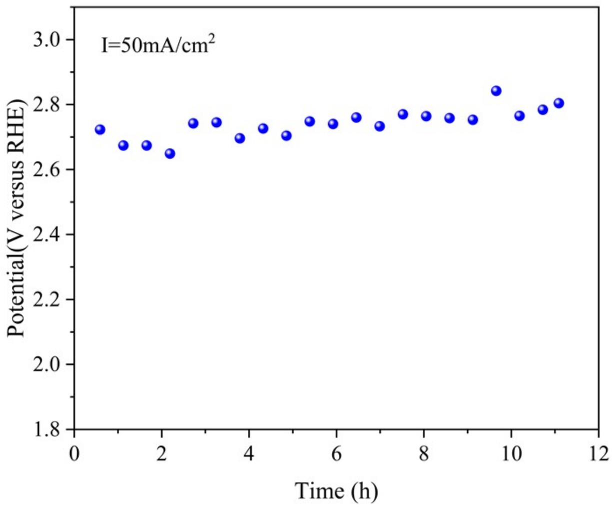

Figure S8 Durability test of ZnFe(3:1)/C-900 at 50 mA cm^{-2}.

Table S4 XPS elemental comparison of catalysts before and after reaction.

Sample	Elemental content (at.%)				
	C	N	O	Fe	Zn
ZnFe(3:1)/C-900-before OER	91.25	2.86	4.93	0.8	0.16
ZnFe(3:1)/C-900-after OER	86.94	0.82	10.09	1.98	0.18
ZnFe(3:1)/C-900- after 15h stability	62.09	2.15	32.66	2.73	0.37

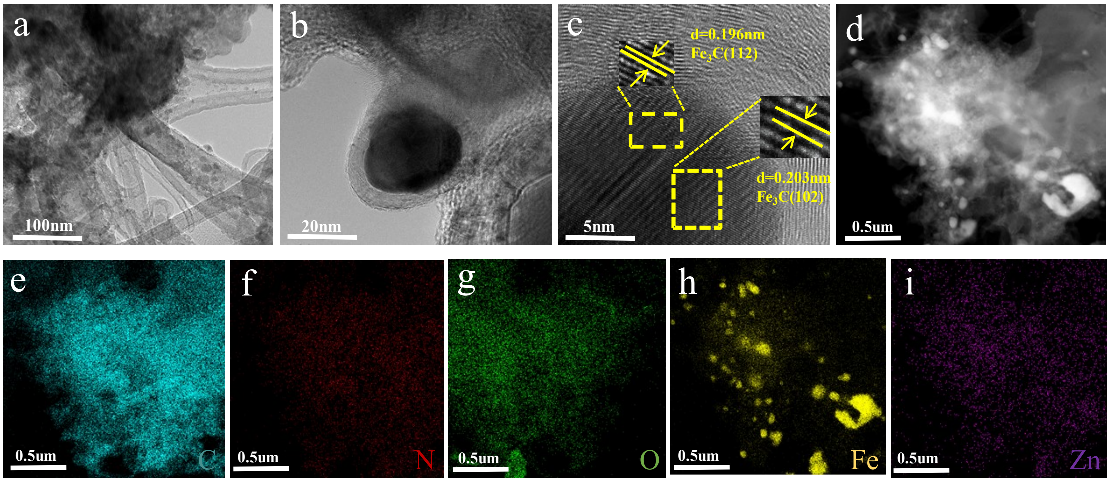

Figure S9 (a-b) TEM images and (c) HR-TEM image of ZnFe(3:1)/C-900-after stability. (d) HAADF-STEM image and (e-i) TEM elemental mappings of the ZnFe(3:1)/C-900-after 15 h stability.

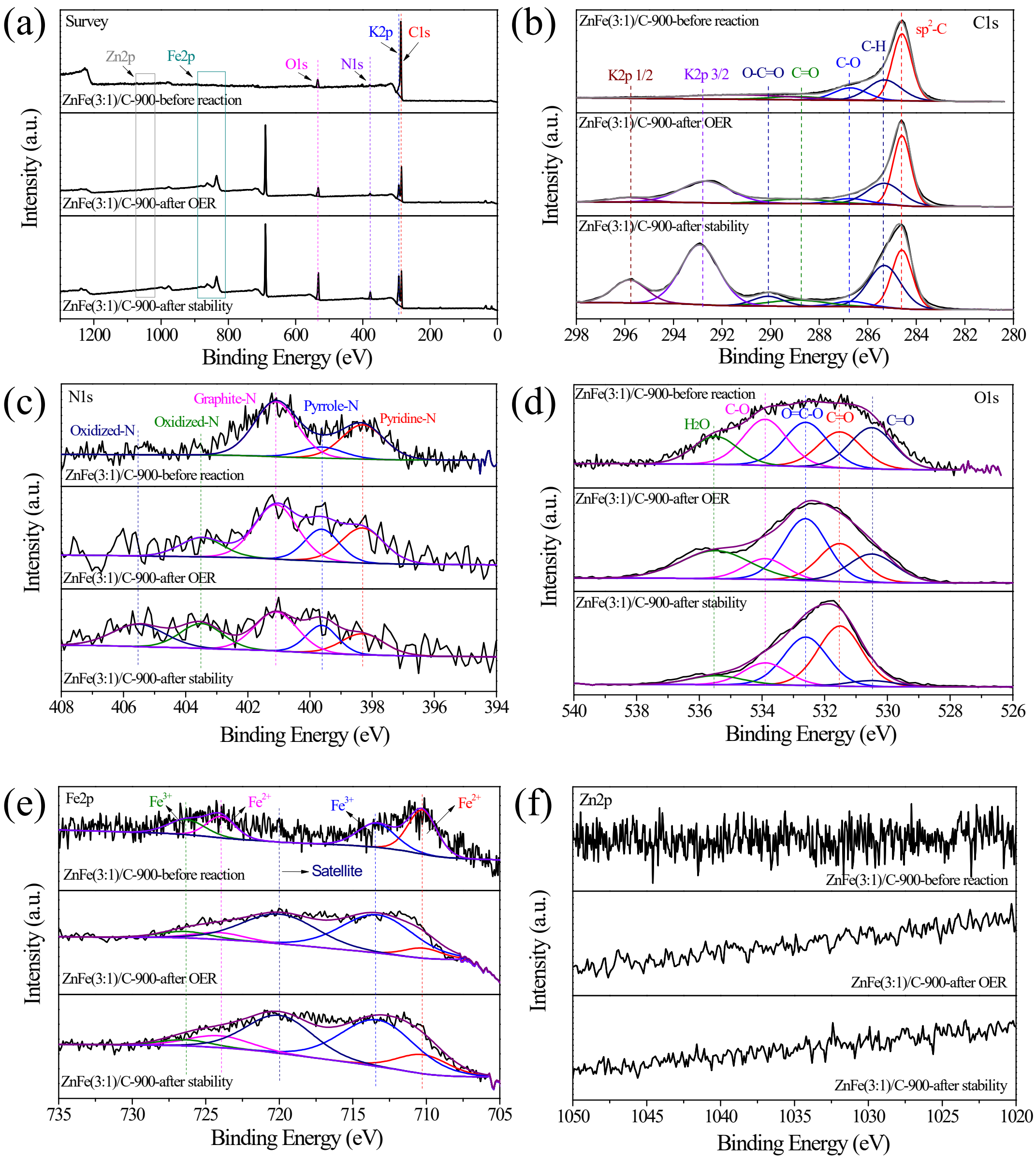

Figure S10 Comparison of XPS survey spectra (a) and high-resolution core-level spectra (C 1s (b), N 1s (c), O 1s (d), Fe 2p (e), Zn 2p (f)) of the ZnFe(3:1)/C-900 catalyst in pre-OER, post-OER, and post-stability testing states.